



Origin of silica and fingerprinting of Australian sedimentary opals



Adriana Dutkiewicz*, Thomas C.W. Landgrebe, Patrice F. Rey

Earthbyte Group, School of Geosciences, University of Sydney, Sydney, NSW 2006, Australia

ARTICLE INFO

Article history:

Received 27 February 2013

Received in revised form 20 October 2013

Accepted 31 October 2013

Available online 27 November 2013

Handling Editor: A.S. Collins

Keywords:

Opal

Great Artesian Basin

LA ICP-MS

Cretaceous

Multivariate analysis

ABSTRACT

Opal is Australia's national gemstone with a significant fraction of the global supply mined from highly weathered Cretaceous sedimentary rocks within the Great Artesian Basin. Surprisingly, relatively little is known about the petrography and trace elemental composition of opal and its host rocks and consequently about the source of silica that underpins its formation. Using laser ablation-inductively coupled plasma mass spectrometry (LA-ICP-MS) of precious and common opal from key opal mining areas in the Great Artesian Basin coupled with multivariate analyses of 59 detectable elements in opal, we show that a mining region from which an opal originates can be constrained by using a combination of Hf, Ba, Zr and Gd with a high degree of confidence. Likewise, precious opal can be distinguished from common (non-precious opal) using a combination of Bi, Ta, Sn and Ca as these particular elements are especially low in concentration in precious opal. Although the opal from the Great Artesian Basin is sedimentary, the Ba content of opals from the eastern part of the basin suggests a volcanic origin. The most likely source of Ba and hence of silica for these opals are feldspars, now altered to kaolinite, sourced as volcanoclastic sediment from the Cretaceous Whitsunday Volcanic Province that marked the rifting and breakup of eastern Gondwana. The alteration of detrital feldspars to kaolinite and their replacement by void-filling opal confirms that weathering has played a critical role in the formation of Australian opal. The opal host rocks are severely weathered with a chemical index of alteration (CIA) up to 92. For the majority of opals studied, the silica is most likely derived locally from the opal host rocks, which impart a unique elemental signature on the opal at any particular locality. Mintabie opal, however, has very low Zr/Hf ratio, which is decoupled from its host rock, suggesting that the silica source is different from all the other opals, or that the silica fluid has experienced intense trace element fractionation, or both. The combination of analytical and statistical methods used here provides a powerful tool for a wide range of provenance studies, not just gemstones, where relationships between a large number of major and trace elements are difficult to unravel.

© 2013 International Association for Gondwana Research. Published by Elsevier B.V. All rights reserved.

1. Introduction

Geochemical fingerprinting is critical for the correct identification of the origin of precious gemstones and plays an important part in the prevention of trade in fake and illegal stones, the valuation process as well as in understanding the geological processes under which the gemstones formed. Major and trace elements are known to impart a distinctive chemical signature for many gemstones and their concentrations have been successfully used in studies of diamonds and sapphires (e.g., Guillon and Günther, 2001; Resano et al., 2003) but never for opal. Opal consists of amorphous $\text{SiO}_2 \cdot n\text{H}_2\text{O}$ comprising silica spheres typically ranging from 150 to 400 nm in diameter (Jones et al., 1964; Sanders, 1964), which in precious opal are of similar size and form an ordered network allowing light to diffract into a striking array of rainbow colours (Sanders, 1964) known as play-of-colour. Common opal, which is intimately associated with precious opal, has the same composition but is composed of randomly arranged silica spheres of variable sizes (Sanders, 1964) and is usually dull white, grey or brown in colour.

Opal also contains 1–9 wt.% of water (Segnit et al., 1965) and trace amounts of “impurities” such as Al, Fe and Ti (Gaillou et al., 2008) which are incorporated in the opal by substitution of tetravalent silicon species or as submicroscopic mineral grains during the opal formation process (Erel et al., 2003). Opal is found in sedimentary and volcanic environments (Smallwood et al., 2008) where it forms under low temperature (Iler, 1979) and is commonly referred to as ‘sedimentary opal’ and ‘volcanic opal’. Sedimentary opal is classified as opal-A and volcanic opal is classified as opal-CT based on X-ray diffraction analysis. Other major differences include the degree of crystallinity, water content and density with sedimentary opals being amorphous and containing 4–9% water compared to the slightly crystalline volcanic opals in which the water content is generally 9–18% (Smallwood et al., 2008). The formation of non-opalescent opal-A has also been documented from hot spring environments (e.g., Akahane et al., 2004). Virtually all opal mined in Australia is sedimentary opal-A (Smallwood et al., 2008) with Australia supplying over 95% of the world's precious opal, which to this day is mined privately by minor operators. The opal occurs almost exclusively within Cretaceous sedimentary rocks of the Great Artesian Basin and is mined from a small number of locations (Fig. 1). However, despite a long history of mining and a well-constrained geological

* Corresponding author. Tel.: +61 2 9351 5192; fax: +61 2 9036 6588.
E-mail address: adriana.dutkiewicz@sydney.edu.au (A. Dutkiewicz).

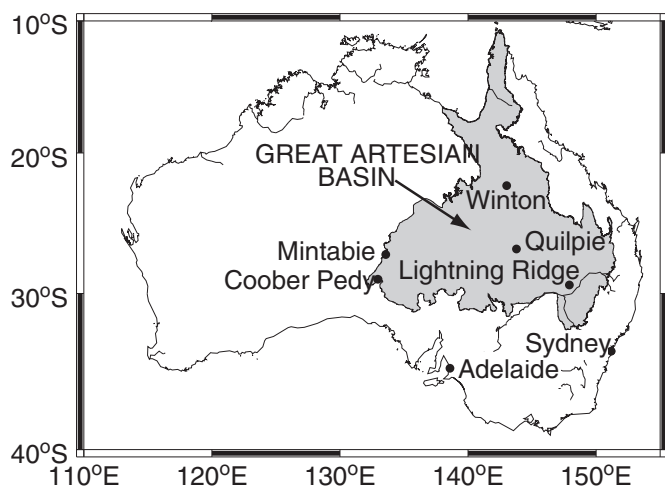


Fig. 1. Present-day extent of the Great Artesian Basin and major opal mining townships.

history of the basin, the formation of sedimentary opal and its uniqueness to the Australian continent are poorly understood (e.g., Merdith et al., 2013). Although the opal has been studied petrographically (Gallacher, 2001), very little is known about the petrology of its host rocks. Likewise the elemental composition of Australian sedimentary opals is poorly documented with only three studies based on inductively coupled plasma mass spectrometry (ICP-MS) conducted to date (Gallacher, 2001; Brown et al., 2004; Gaillou et al., 2008). Here, we have used laser ablation ICP-MS (LA-ICP-MS) on precious and common opal from key opal mining areas in order to constrain the possible sources of silica involved in opal genesis (a critical aspect of opal formation) and to assess whether any elements could be used to determine the provenance of opal with respect to a particular mining area. This approach had proven extremely useful for the fingerprinting of sapphires and diamonds (e.g., Resano et al., 2003) but until now has never been applied to opals.

2. Opal and its host rocks

The Cretaceous sediments, which comprise the host rocks for the opal in the Great Artesian Basin, were deposited from ca. 125 Ma to 95 Ma when an epicontinental sea flooded central Australia (Frakes et al., 1987; Campbell and Haig, 1999) as the Australian plate was moving eastward over a west-dipping subduction zone (Fig. 2) (Matthews et al., 2011). A silicic-dominated large igneous province comprising the Whitsunday volcanics, developed along the eastern Australian margin ca. 132–95 Ma (Fig. 2) marking the onset of continental break-up in eastern Gondwana (Bryan et al., 2000). Much of the volcanogenic material is now preserved within marine and fluvial Cretaceous sedimentary rocks in the Great Artesian Basin and is intimately associated with opal (Fig. 3). The basin experienced a major period of uplift between 100 and 65 Ma with erosion removing a package of sedimentary rock up to 3 km thick (e.g., Raza et al., 2009). Intense weathering resulted in extensive silicification within the Tertiary regolith (Thiry et al., 2006). In Winton and Quilpie (Fig. 1) the opal occurs within the late Albian to Cenomanian fluvial, volcanoclastic Winton Formation (Fig. 3) (Exon and Senior, 1976), which is red–brown ironstone, dominated by goethite and kaolinite mineralogy with minor quartz and illite (Table 1); in Lightning Ridge within late Albian kaolinite-rich (Table 1) Finch Claystone deposited in a flood plain environment; in Coober Pedy within the early Cretaceous kaolinite-rich (Table 1), marine Bulldog Shale (Fig. 3) (Exon and Senior, 1976); in Mintabie within Ordovician fluviodeltatic sandstones of the Mintabie Beds (Fig. 3) (Barnes et al., 1992), the only field that has produced opal from Paleozoic rocks. The mineralogy of the Bulldog Shale and Finch Claystone is broadly similar

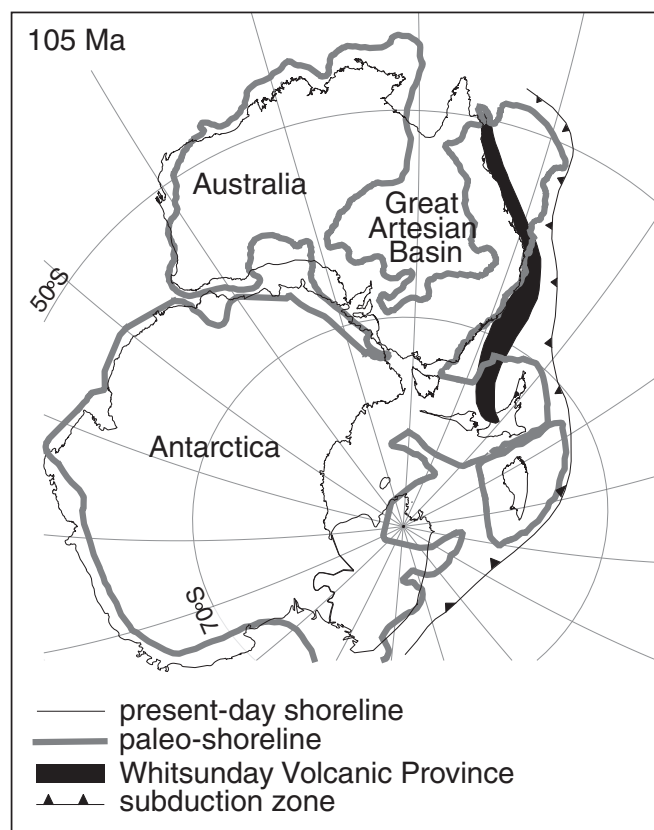


Fig. 2. Configuration of the Australian plate at 105 Ma showing the position of the paleo-shorelines (Golonka, 2007) and silicic large igneous province cluster comprising the Whitsunday Volcanic Province (Bryan and Ernst, 2008).

in that it is dominated by kaolinite, followed by quartz with smectite and illite comprising a relatively minor component of the clay fraction (Table 1). All opal host rocks contain a significant amorphous fraction (up to 63%; Table 1), which is attributed to opaline silica. The opal frequently occurs as cm to dm-thick bands or pockets at the interface between shale and sandstone (Barnes et al., 1992) filling primary and secondary pore spaces and fractures (Fig. 4) and is usually found down to 30 m below the surface. In our samples, the opal shows a variety of colours ranging from blue to green to red for precious opal and white to grey and brown for non-precious or common opal. Australian sedimentary opal has never been dated radiometrically due to its low U content (Gaillou et al., 2008) so its age can only be estimated using the age of the host rocks (Exon and Senior, 1976; Thiry et al., 2006), associated minerals (Newberry, 2004), formation of silcrete (Senior and Mabbutt, 1979; Thiry et al., 2006) and carbon inside cracks in opal (Dowell et al., 2002). Thus the age of the opal varies from 130 Ma to 1 kyr B.P., which could reflect a poor selection of material used in dating or alternatively, multiple phases of opal genesis.

3. Methodology

3.1. X-ray diffraction analysis

Three key samples, one from each major opal-hosting stratigraphic horizon, were analysed by X-ray diffraction (XRD) in order to determine the composition of the fine fraction (Table 1). Based on visual examination of hand specimens as well as polished sections, the host rock from Coober Pedy is similar to the host rock from Mintabie in terms of the fine fraction, while the Winton host rock is similar to the host rock in Quilpie. The Lightning Ridge host rock is slightly different in appearance from host rocks in South Australian and Queensland opal mining

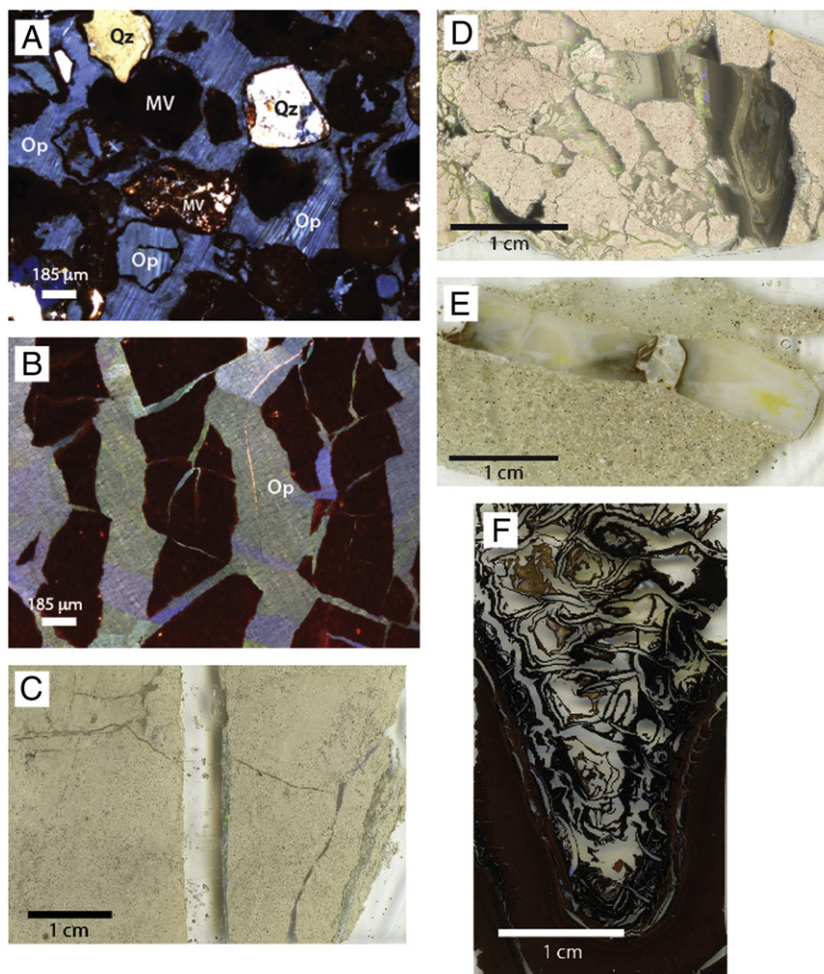


Fig. 3. Photomicrographs and polished section scans showing textural relationships between opal and its host rock. A–B polarised light. C–F slide scans. A) Common opal (Op) filling all intergranular and intragranular porosity within the host Winton Formation, Quilpie. Note the abundance of well-rounded mafic volcanic rock fragments (MV) and detrital quartz grains (Qz). B) Precious opal within highly fractured matrix dominated by goethite–kaolinite mineralogy, Winton Formation, Quilpie. C) A vein of opal within Bulldog Shale host rock, Coober Pedy. D) Banded opal with flow structures within Finch Claystone, Lightning Ridge. E) Vein opal within sandy Mintabie Beds, Mintabie. F) Boxwork structure hosting opal within iron-rich Winton Formation, Quilpie.

regions and this is confirmed by the XRD analysis. XRD patterns were recorded with a PANalytical X'Pert Pro Multi-purpose Diffractometer using Fe filtered Co K α radiation, automatic divergence slit, 2° anti-scatter slit and fast X'Celerator Si strip detector. The diffraction patterns were recorded in steps of 0.017° two theta with a 0.5 second counting time per step, and logged to data files for analysis. Quantitative analysis was performed on the XRD data using the commercial packages TOPAS (Bruker AXS) and SIROQuant (Sietronics Pty Ltd) at CSIRO in Adelaide. The results are given in Table 1.

3.2. LA-ICP-MS analysis of opal

Using LA-ICP-MS we analysed 123 spots, each comprising 59 detectable major and trace elements on mostly vein opal on 5 key samples from Quilpie, Mintabie, Lightning Ridge and Coober Pedy mining areas (Fig. 1). Approximately 50 analyses that partially sampled the host

matrix or solid inclusions within the opal were discarded. The key samples were selected from a total of about 200 with a focus on specimens that contain abundant opal located in veins or fractures, are visually typical of the mining area in terms of host rock composition (Fig. 3) but that at the same time show great petrographic variability on a microscopic scale. These variabilities include opal colour, which within a single sample may include blue, green, orange, red, white, brown and various shades of grey indicating intergrowth of precious and common opal, as well as microstructure including evidence for multiple fracture events, flow and meniscus structures and boxwork textures (Fig. 3) that may result in variable concentrations of particular elements at microscopic scale. Consequently, our approach was to thoroughly analyse variabilities in element content in opal in individual samples rather than focus on one or two analyses in a large suite of opals from different regions that simply would not capture this variability. It is worth noting that the field areas are spread over large distances (hundreds of

Table 1
Quantitative XRD analysis (wt.%) of opal host rocks from Coober Pedy (CP_4), Winton (W_2) and Lightning Ridge (LR_4).

Sample name	Lithology	Formation name	Goethite	Kaolinite	Quartz	Smectite	Illite	Amorphous
CP_4	Shale	Bulldog Shale	<1	34	15	4	1	46
W_2	Ironstone	Winton Formation	41	13	7	nd	2	36
LR_4	Claystone	Finch Claystone	<1	17	13	5	2	63

nd – not detected; amorphous component is most likely amorphous opaline silica.

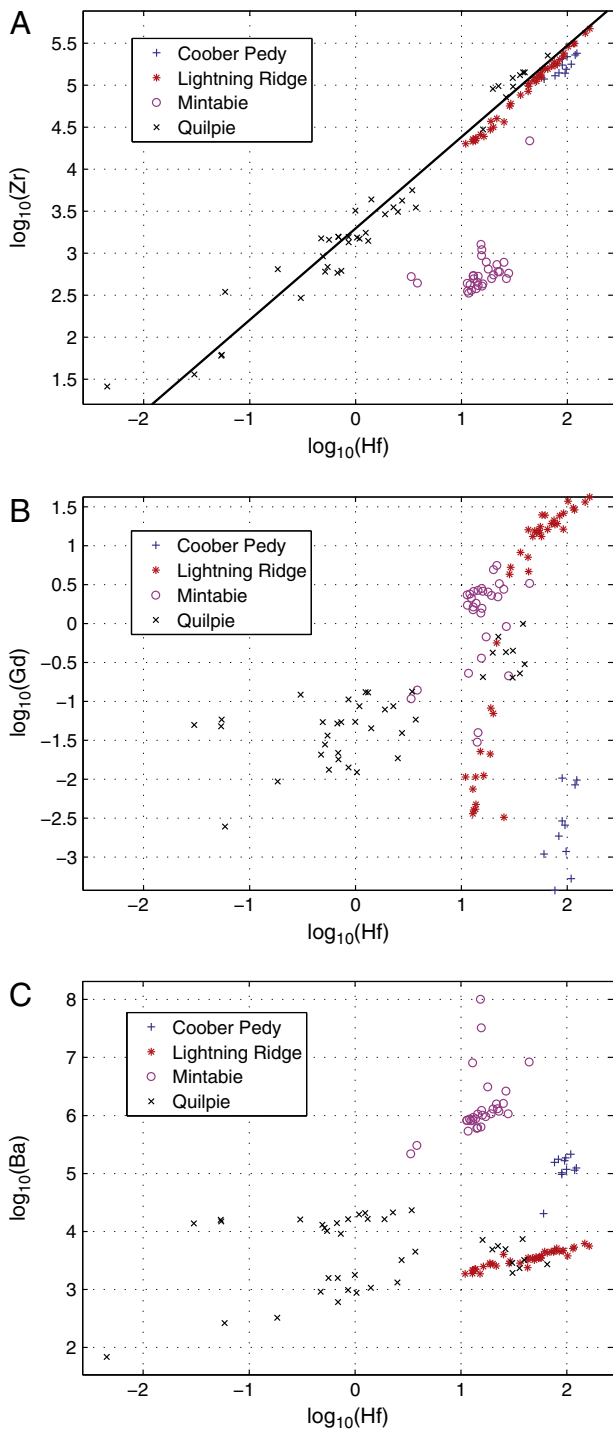


Fig. 4. Distributions of elements that best discriminate opal mining regions based on multivariate analysis. Note that the Zr and Hf content of opals from Coober Pedy, Lightning Ridge and Quilpie is near chondritic and can be approximated by a linear regression.

kilometres) and that the opal host rocks are distinctly different in terms of colour and composition (Fig. 3). The analyses were conducted using Agilent 7500s ICP-MS and Resonetics M50 Excimer laser at CODES, University of Tasmania (Guillong et al., 2011). Ablation was performed at CODES on the University of Tasmania's Agilent 7500s ICP-MS with a Resonetics M50 Excimer laser in an atmosphere of pure He. Spot size was generally 35 μm , the energy beam was 3.5 J/cm² and the laser pulse frequency 5 Hz and the polished sections ~ 120 μm -thick. Synthetic glass (NIST612 from the National Institute of Standards and Technology and GSD-1G from the United States Geological Survey) was used

as primary and secondary standard reference material with Si as an internal standard to correct for ablation yield and instrument drift. Based on the analysis of the secondary reference material, the accuracy of the LA-ICP-MS techniques was found to be within 3–5%. Further information on instrumental parameters can be found in Müller et al. (2009) and Guillong et al. (2011). Diagnostic element contents of opal from Lightning Ridge, Coober Pedy, Mintabie and Quilpie are given in Table 2.

3.3. ICP-MS analysis of host rocks

Ten representative host rocks were bulk analysed using ICP-MS by Australian Laboratory Services Pty. Ltd. (Table 3). The samples were powdered using a tungsten carbide mill. The H₂O content and loss on ignition were determined by multi-temperature thermogravimetric analyser (TGA), the silicate content was determined by inductively coupled plasma atomic emission spectroscopy (ICP-AES) following lithium borate fusion and acid dissolution. The Ca and Ba contents were determined by ICP-MS following lithium borate fusion and acid dissolution. The chemical index of alteration (CIA) was calculated using the relationship.

$$\text{CIA} = [\text{Al}_2\text{O}_3 / (\text{Al}_2\text{O}_3 + \text{CaO}^* + \text{Na}_2\text{O} + \text{K}_2\text{O})] \times 100$$
 of Nesbitt and Young (1982) where CaO* is the amount of CaO incorporated in the silicate fraction of the rock. As no carbonate, apatite nor gypsum were detected nor observed in the sample, this correction was not applied.

3.4. Statistical analysis

Given the vast amount of geochemical data collected on each sample (7257 data points) and no prior studies on how different groupings of elements co-vary in different opals, a statistical analysis was undertaken in order to identify combinations of elements that are diagnostic of both the opal type (common versus precious) and mining locality of opal. For opal type, it is of interest to ascertain which elements reflect the differences between common and precious opal, whereas for opal mining locality, obtaining an ensemble of elements useful for “fingerprinting” locality is the objective. A statistical approach was used to explicitly factor in inherent variabilities in chemistry across different categories, and to summarise significant differences for a large number of variables (i.e., each element). The methodology utilises a quantitative approach involving multivariate feature ranking (Liu and Motoda, 1998) in order to rank/select important major and trace elements useful for these discriminations.

The feature ranking methodology entails ranking the various elements according to their multivariate separabilities (i.e., statistical uniqueness) in terms of category (i.e., an element with a large degree of separation between categories would obtain a high rank). Feature ranking involves gradually selecting combinations of elements, and testing the resultant separation between categories. A criterion is required to quantify this degree of separability. In this study, the separability is based on a multivariate linear discriminant analysis (which takes both the separation within and between categories into account). This approach has the advantage of selecting elements that are not only discriminative, but are also more statistically independent of other elements (univariate approaches cannot distinguish the fact that elements may be correlated, resulting in redundancy).

In an attempt to prevent over-fitting, the feature ranking analyses were undertaken using a 20-fold randomised hold-out procedure, where 70% of data was randomly selected for optimising the ranking, followed by the remaining data used as a validation dataset. The twenty results were then analysed for consistency, with the elements calculated to be consistently of the highest ranks reported. The Matlab statistics toolbox was used for the experiments, and the Matlab code is provided for repeatability (see Supplementary Data). The four most discriminative elements were extracted in each experiment. Since the dataset used in this study is relatively small, the study also involved plotting

pair-wise combinations of high-ranked elements, allowing the various data distributions between categories to be visualised. This aids the assessment of the analysis empirically, with an inspection of the resultant distribution providing an additional measure of confidence.

4. Results and discussion

4.1. Opal fingerprinting

The elemental composition of Australian opals is poorly documented. Brown et al. (2004) used LA-ICP-MS to determine the relationship between transition elements and opals of different colours. They found that darker opals contain higher concentrations of these elements compared to lighter opals. In their elemental studies of opal Brown et al. (2004) and Gaillou et al. (2008), using bulk ICP-MS, both concluded that there is no relationship between the composition of Australian opals and their locality. In this study, by using multivariate feature-selection analysis of concentrations of all detectable elements in five opal samples from four different locations we show that the mining region from which the opals originate can be discriminated. This can be done with just 4 elements from a suite of 59 with the best discriminators based on multivariate analysis being Zr, Hf, Gd and Ba (Table 2). This combination of elements is particularly useful for distinguishing Mintabie, Quilpie and Coober Pedy opals from each other with good separability of Quilpie and Mintabie localities occurring in Hf–Zr space (Fig. 4A) and separability of Coober Pedy opals from other opals occurring in Hf–Ba space (Fig. 4C). Lightning Ridge opal overlaps with Coober Pedy and Quilpie opals in Hf–Zr space but shows better separability in Hf–Gd space (Fig. 4B) where it shows partial overlap with Mintabie and Quilpie opals but no overlap with Coober Pedy opals. In contrast, Lightning Ridge opal shows good separability from Mintabie and Coober Pedy opals in Hf–Ba space but instead overlaps with Quilpie opals (Fig. 4C). Consequently, the Lightning Ridge opals can only be distinguished from the other mining areas by using a combination of Hf, Gd and Ba. The Quilpie opal shows by far the lowest concentrations of Hf (mostly 0.1 to 1.77 ppm). The highest levels of Hf (5 to 9 ppm) are found in the Lightning Ridge and the Mintabie opal samples. The concentration of Ba suggests distinct clustering of opal mining localities and is highest in Mintabie opal (~210–3000 ppm), followed by Coober Pedy opal (146–207 ppm) and Lightning Ridge opal (26–44 ppm). The Quilpie opal sample has the most variable Ba content but generally falls into two discrete clusters of very low (6–26 ppm) and moderate (47–79 ppm) concentrations overlapping with concentrations found in Lightning Ridge opals. The Gd content is highest for Lightning Ridge common opals (2–5 ppm), followed by Mintabie opals, which form a distinct cluster around 1–2 ppm, followed by Quilpie opals clustering around 0.13–1.14 ppm of Gd and the lowest values recorded in Coober Pedy opals (<0.13 ppm) showing a partial overlap with low concentrations found in precious opal from Lightning Ridge (Table 2). The opals display a wide range of Zr concentrations with some of the highest values (up to about 290 ppm obtained from Lightning Ridge, Coober Pedy opals and significantly lower values obtained from Mintabie and Quilpie opals (mainly clustered around 10–40 ppm).

None of these elements allow the discrimination between precious and common opal; however, these can be distinguished using a combination of Ta, Bi, Sn and Ca (Fig. 5) as all of these elements, with the exception of Ca, are in relatively low concentrations in precious opals compared to common opals where the concentration of these elements is higher by a degree of magnitude (Table 2). This is consistent with neutron activation analysis of opals (McOrist and Smallwood, 1997). Precious opal colour (red vs green vs blue) is very difficult to discriminate based on elemental content and this likely reflects the dependence of colour on the nanostructure of opal (Sanders, 1964) rather than on impurities. Opal fingerprinting is therefore possible using just a small number of key elements.

4.2. Elemental composition and source of silica

Using bulk ICP-MS Gaillou et al. (2008) concluded that Australian sedimentary opals (opal-A in sedimentary rocks; Smallwood et al. (2008)) have elemental characteristics that are distinctly different from “volcanic” opals (higher temperature opal-CT in volcanic rocks; Smallwood et al. (2008)) and that they can be distinguished based on their Ba (Ba content of volcanic opal is <110 ppm, Ba content of sedimentary opal is >110 ppm) and Ca contents. However, our study indicates that even though opals from the Great Artesian Basin are all classified as sedimentary, many show Ba concentrations consistent with a volcanic origin (Fig. 6) suggesting that silica fluids from which they formed were derived from a volcanic source. This is true for our analysis of all opals from Lightning Ridge and Quilpie and some opals from Coober Pedy. Only Mintabie opal, which is hosted in Ordovician sandstone, shows Ba concentrations well in excess of 110 ppm consistent with a sedimentary classification. Interestingly, the volcanic opals from the Wollo Province in Ethiopia have a Ba content of 82–226 ppm (Rondeau et al., 2010) overlapping with that of sedimentary opal suggested by Gaillou et al. (2008). Ba is a minor but notable component of feldspars (Milliken, 1989) and is released into pore fluids during weathering; the more weathering that has occurred, the more enriched in Ba will be the silica fluids from which the opal forms (Gaillou et al., 2008). The most likely source of Ba for the majority of studied opals is the Cretaceous Whitsunday Volcanic Province (Bryan et al. (2000); Fig. 2), which supplied vast amounts of volcanogenic material into the Great Artesian Basin estimated to comprise as much as 1×10^6 km³ of volcanogenic sedimentary material filling the Great Artesian Basin (Bryan et al., 1997). Consequently, opal fields that are located close to this province (Quilpie, Lightning Ridge; Fig. 1) show the lowest concentrations of Ba compared to Coober Pedy opals located further away and in older rocks that have been subjected to weathering over a longer period of time (Mintabie; Fig. 1). The weathering of feldspars from the volcanoclastic rocks would have provided ample silica-rich fluids for the formation of opal. This source of silica is supported by petrographic evidence where reworked feldspar grains have been completely dissolved and replaced by opal while neighbouring mafic volcanic fragments and detrital quartz have remained unscathed (Fig. 3). It is also supported by the abundance of kaolinite (up to 34%; Table 1), a major alteration product of feldspars (Nesbitt and Young, 1984), within the opal host rocks. All the opal host rocks have experienced extensive weathering with CIA values ranging from 63.3 (Mintabie Beds) to 91.5 (Winton Formation) (Table 3) and are consistent with values obtained for alluvial sediments in the Great Artesian Basin (Kamber et al., 2005). The silica source for the formation of opal at Mintabie appears to be different from all the other opals. The Hf and Zr concentrations for Mintabie opal form a discrete cluster (Fig. 4A) that unlike opals from Quilpie, Lightning Ridge and Coober Pedy show a substantial deviation from chondritic values (Jochum et al., 1986). Zr/Hf ratios are unusually low with an average value of 5.4 for Mintabie opal compared to opal from Quilpie (average = 28.7), Lightning Ridge (average = 28.0) and Coober Pedy (average = 28.8). Such low values have been found in some granites (Irber, 1999; Zarausky et al., 2009), reflecting crystallisation and removal of zircon in the crust and effective melt segregation (Claiborne et al., 2006), as well as in late crystallising zircons and hydrothermal zircons (Wang et al., 2010). In addition, the Mintabie opal Zr/Hf ratios differ substantially from those of its host rock (Mintabie Beds), which are 33.5 and 35.2 for the two samples analysed (Table 3) and are consistent with values obtained for Mesoproterozoic Gawler Range Volcanics (Schaffer, pers. comm., February 2013). These ratios are slightly lower than chondritic values (36.6; Jochum et al., 1986) and are similar to Zr/Hf ratios obtained for Bulldog Shale, Winton Formation and Finch Claystone that host all other major opal deposits within the Great Artesian Basin. Zr and Hf are relatively immobile during sedimentary processes and are considered to be reliable indicators of provenance (Taylor and McLennan, 1985). This suggests that silica

Table 2

Selected element content (ppm) of P and C opal hosted in veins (Lightning Ridge (LR), Coober Pedy and Mintabie) and boxwork texture (Quilpie) from key mining areas from the Great Artesian Basin determined by LA-ICP-MS. P = precious opal, C = common opal.

Sample name	Location	Opal colour	Opal type	Ca	Zr	Sn	Ba	Gd	Hf	Ta	Bi
N36443	LR	Blue	P	711	76.1	0.0861	26.5	0.119	3.03	0.0518	0.0128
N36443	LR	Green	P	631	76.7	0.133	28.4	0.0919	3.10	0.0547	<0.0125
N36443	LR	Medium grey	C	773	147	0.433	34.7	1.95	5.13	0.189	0.0914
N36443	LR	Orange–red	P	656	79.1	0.109	28.5	0.139	3.11	0.0656	0.0165
N36443	LR	Green	P	623	82.6	0.207	26.4	0.193	3.25	0.0826	0.0268
N36443	LR	Medium grey	C	752	180	0.586	37.8	3.36	6.13	0.273	0.1670
N36443	LR	Green	P	702	78.5	0.108	28.5	0.0980	3.12	0.0641	<0.0087
N36443	LR	Blue	P	635	73.9	0.113	26.3	0.139	2.83	0.0545	0.0108
N36443	LR	Blue	P	692	78.2	0.150	28.1	0.0867	3.03	0.0524	0.0159
N36443	LR	Green	P	663	77.4	0.171	28.0	0.0909	3.05	0.0650	0.0086
N36443	LR	Medium grey	C	716	80.7	<0.0834	29.8	0.142	3.36	0.0658	0.0154
N36443	LR	Medium grey	C	759	87.4	0.0929	31.7	0.187	3.57	0.0701	0.0147
N36443	LR	Medium grey	C	694	96.5	0.222	30.8	0.337	3.59	0.108	0.0247
N36443	LR	Medium grey	C	804	244	1.26	41.7	4.32	7.90	0.377	0.247
N36443	LR	Medium grey	C	704	163	1.93	33.4	3.29	5.44	0.254	0.426
N36443	LR	Medium grey	C	701	164	1.84	34.5	3.32	5.66	0.260	0.405
N36443	LR	Light grey	C	720	162	1.95	34.5	3.06	5.79	0.245	0.406
N36443	LR	Medium grey	C	733	202	0.746	38.7	4.00	6.87	0.328	0.192
N36443	LR	Medium grey	C	722	186	0.838	38.5	3.62	6.37	0.306	0.201
N36443	LR	Medium grey	C	822	291	1.70	42.5	5.09	9.13	0.485	0.377
N36443	LR	Light grey	C	789	210	1.21	39.3	3.37	7.12	0.347	0.249
N36443	LR	Medium grey	C	681	100	0.384	30.1	0.779	3.79	0.115	0.0610
N36443	LR	Medium grey	C	690	168	1.20	35.0	3.20	5.70	0.262	0.294
N36443	LR	Light grey	C	729	156	1.62	35.1	3.23	5.51	0.229	0.363
N36443	LR	Light grey	C	742	177	1.93	36.1	4.04	5.82	0.263	0.410
N36443	LR	Light grey	C	779	169	2.03	34.8	3.47	5.72	0.258	0.445
N36443	LR	Medium grey	C	663	132	1.28	31.6	2.50	4.75	0.187	0.283
N36443	LR	Light grey	C	598	138	1.58	29.3	2.35	5.09	0.204	0.303
N36443	LR	Light grey	C	761	218	2.81	39.1	4.12	7.13	0.347	0.658
N36443	LR	Light grey	C	750	235	3.11	35.9	4.82	7.45	0.367	0.707
N36443	LR	Light grey	C	733	152	1.70	33.6	3.34	5.12	0.221	0.345
N36443	LR	Medium grey	C	693	116	0.853	31.5	1.89	4.28	0.139	0.177
N36443	LR	Light grey	C	694	156	1.45	34.5	3.06	5.33	0.248	0.311
N36443	LR	Light grey	C	757	188	0.936	39.3	3.58	6.57	0.309	0.171
N36443	LR	Medium grey	C	773	192	0.952	40.8	3.62	6.71	0.313	0.190
N36443	LR	Light grey	C	773	244	1.17	40.6	4.42	7.82	0.396	0.263
N36443	LR	Green	P	759	90.0	0.185	31.3	0.315	3.68	0.0897	0.0137
N36443	LR	Light grey	C	776	196	0.856	38.4	3.77	6.52	0.325	0.1625
N36443	LR	Medium grey	C	799	181	1.99	38.5	4.02	5.98	0.262	0.4194
N36443	LR	Dark grey	C	688	119	1.24	32.8	2.06	4.33	0.155	0.2846
N36443	LR	Green	P	890	96.1	0.132	36.8	0.0829	4.06	0.0725	<0.0216
N36443	LR	Medium grey	C	819	276	1.541	44.3	4.77	8.75	0.473	0.332
CP-2	Coober Pedy	Dark grey	C	1571	180	0.141	194	0.0533	7.30	0.174	<0.0116
CP-2	Coober Pedy	Dark grey	C	1591	191	<0.0778	207	0.0377	7.67	0.187	<0.0083
CP-2	Coober Pedy	Dark grey	C	556	160	0.071	74.4	0.0518	5.92	0.122	<0.0088
CP-2	Coober Pedy	Green	P	1522	172	0.119	190	0.0650	6.83	0.194	<0.0069
CP-2	Coober Pedy	Green	P	1445	166	<0.0752	180	0.0325	6.57	0.173	<0.0044
CP-2	Coober Pedy	Blue	P	1385	171	0.100	185	0.0750	7.23	0.186	0.0073
F-tray	Coober Pedy	Light–med. grey	C	1554	189	0.148	146	0.0791	7.04	0.190	<0.0157
F-tray	Coober Pedy	Light–med. grey	C	1359	208	<0.1210	160	<0.0858	7.37	0.214	<0.0129
F-tray	Coober Pedy	Light–med. grey	C	1128	213	<0.1516	157	0.126	7.95	0.215	<0.0188
F-tray	Coober Pedy	Light–med. grey	C	1324	204	<0.1928	150	0.137	7.04	0.215	<0.0148
F-tray	Coober Pedy	Light–med. grey	C	1333	217	<0.2650	164	0.134	8.07	0.214	<0.0172
Mintabie-4	Mintabie	Light grey	C	1017	12.5	0.892	309	0.530	2.91	0.701	0.0959
Mintabie-4	Mintabie	Brown–red	C	1169	22.4	4.26	2994	1.15	3.27	0.508	0.479
Mintabie-4	Mintabie	Brown–red	C	1318	76.8	6.85	1016	1.68	5.18	0.628	0.747
Mintabie-4	Mintabie	Brown–red	C	1218	21.0	3.50	1829	1.58	3.29	0.593	0.622
Mintabie-4	Mintabie	White	C	677	14.1	3.50	242	0.4258	1.79	0.155	0.0707
Mintabie-4	Mintabie	Light grey	C	1019	15.5	2.23	373	1.24	3.04	0.626	0.381
Mintabie-4	Mintabie	Light grey	C	636	15.2	3.38	208	0.381	1.69	0.162	0.0653
Mintabie-4	Mintabie	Light grey	C	1039	12.8	1.60	373	1.27	2.88	0.546	0.378
Mintabie-4	Mintabie	Light grey	C	1087	15.3	1.70	1003	1.20	3.03	0.587	0.416
Mintabie-4	Mintabie	Medium grey	C	1089	13.0	1.33	369	1.39	2.99	0.624	0.398
Mintabie-4	Mintabie	Light grey	C	1028	14.1	1.50	371	1.45	2.88	0.579	0.397
Mintabie-4	Mintabie	Medium grey	C	1173	14.8	1.43	391	1.51	3.05	0.576	0.419
Mintabie-4	Mintabie	Light grey	C	1045	15.3	1.56	414	1.54	3.18	0.624	0.416
Mintabie-4	Mintabie	Medium grey	C	1005	13.8	1.46	380	1.46	2.95	0.586	0.415
Mintabie-4	Mintabie	Light grey	C	1078	14.0	1.22	406	1.52	3.33	0.665	0.365
Mintabie-4	Mintabie	Light grey	C	1094	15.5	1.51	451	2.00	3.68	0.681	0.507
Mintabie-4	Mintabie	Light grey	C	1209	16.7	1.95	663	1.50	3.50	0.677	0.429
Mintabie-4	Mintabie	Med.–dark grey	C	965	13.2	1.23	382	1.30	3.13	0.591	0.382
Mintabie-4	Mintabie	Dark grey & brown	C	1188	17.6	2.35	493	2.11	3.80	0.785	0.626
Mintabie-4	Mintabie	Light grey	C	1139	13.6	1.15	442	1.22	3.30	0.605	0.318
Mintabie-4	Mintabie	Brown	C	1273	14.9	2.36	616	0.966	4.16	0.640	0.393

(continued on next page)

Table 2 (continued)

Sample name	Location	Opal colour	Opal type	Ca	Zr	Sn	Ba	Gd	Hf	Ta	Bi
Mintabie-4	Mintabie	White	C	1268	18.1	1.76	397	0.845	3.44	0.353	0.0627
Mintabie-4	Mintabie	Med.-dark grey	C	1109	13.7	1.33	327	0.247	3.18	0.326	0.0202
Mintabie-4	Mintabie	Light grey	C	1030	19.6	2.38	332	0.643	3.29	0.248	0.0738
Mintabie-4	Mintabie	White	C	1006	14.3	1.15	323	0.218	3.16	0.255	0.0301
Mintabie-4	Mintabie	Light grey	C	1325	15.9	1.45	417	0.513	4.24	0.853	0.143
Mintabie-4	Mintabie	Light grey	C	1234	16.2	1.23	453	1.41	3.84	0.717	0.351
Mintabie-4	Mintabie	Dark grey	C	1176	16.1	1.24	436	1.67	3.90	0.746	0.415
Mintabie-4	Mintabie	Yellow-brown	C	1249	18.1	1.45	498	1.56	4.06	0.801	0.505
Mintabie-4	Mintabie	Light grey	C	1101	14.9	1.37	416	1.44	3.61	0.708	0.398
Q-1	Quilpie	Blue	P	561	16.3	0.271	52.4	0.282	0.87	0.0369	0.0329
Q-1	Quilpie	Blue	P	741	17.1	<0.0985	55.0	0.237	0.77	0.0310	0.0200
Q-1	Quilpie	Light grey	C	850	25.6	0.225	75.1	0.414	1.10	0.0560	0.0810
Q-1	Quilpie	Light grey	C	810	23.9	0.214	73.2	0.346	1.04	0.0471	0.0651
Q-1	Quilpie	Light grey	C	729	23.2	0.136	67.8	0.412	1.13	0.0548	0.0515
Q-1	Quilpie	Light grey	C	754	22.9	0.158	67.3	0.377	0.938	0.0499	0.0500
Q-1	Quilpie	Dark grey	C	636	5.9	0.083	66.7	0.267	0.281	0.0124	0.0117
Q-1	Quilpie	Dark grey	C	684	11.8	0.342	67.3	0.400	0.596	0.0373	0.0291
Q-1	Quilpie	Dark grey	C	663	4.7	0.101	62.8	0.272	0.218	0.0142	<-0.0099
Q-1	Quilpie	Dark grey	C	761	6.0	<0.123	64.9	0.291	0.283	0.0152	0.0139
Q-1	Quilpie	Light grey	C	667	42.5	0.228	78.8	0.418	1.70	0.0933	0.125
Q-1	Quilpie	Light grey	C	629	34.7	0.132	75.7	0.346	1.43	0.0706	0.113
Q-1	Quilpie	Light grey	C	585	32.0	0.230	67.5	0.332	1.32	0.0731	0.0890
Q-1	Quilpie	Dark grey	C	470	19.4	<0.106	61.3	0.282	0.734	0.0442	0.0618
Q-1	Quilpie	Dark grey	C	474	16.1	0.0899	58.1	0.211	0.749	0.0252	0.0363
Q-1	Quilpie	Dark grey	C	594	15.9	0.133	63.1	0.277	0.843	0.0192	0.0176
Q-1	Quilpie	White	C	251	23.6	0.247	24.5	0.153	0.778	0.0518	0.0746
Q-1	Quilpie	Light grey	C	379	33.4	0.212	25.8	0.283	0.997	0.0677	0.0684
Q-1	Quilpie	Medium grey	C	227	24.5	0.135	24.4	0.190	0.849	0.0504	0.100
Q-1	Quilpie	Light grey	C	184	24.0	0.090	19.4	0.186	0.723	0.0570	0.0789
Q-1	Quilpie	Light grey	C	240	12.7	0.309	11.3	0.0735	0.292	0.0176	0.0900
Q-1	Quilpie	Light grey	C	279	16.6	0.935	12.3	0.131	0.479	0.0393	0.111
Q-1	Quilpie	Light grey	C	274	4.1	0.271	6.3	<0.0361	0.0958	0.0106	0.0142
Q-1	Quilpie	Medium grey	C	262	24.3	0.276	18.9	0.148	1.01	0.0474	0.0574
Q-1	Quilpie	Medium grey	C	270	24.4	0.183	16.2	0.175	0.851	0.0493	0.0673
Q-1	Quilpie	Medium grey	C	217	24.4	0.0760	19.9	0.157	0.935	0.0447	0.0704
Q-1	Quilpie	Medium grey	C	596	87.7	0.349	47.2	0.502	3.33	0.160	0.152
Q-1	Quilpie	Dark grey	C	535	37.7	<0.0848	33.3	0.245	1.55	0.0658	0.0445
Q-1	Quilpie	Dark grey	C	563	34.6	<0.250	38.6	0.291	1.77	0.0435	0.291
Q-1	Quilpie	Light grey-white	C	1734	173	3.25	33.3	0.592	4.94	0.597	0.126
Q-1	Quilpie	Medium grey	C	1540	162	3.13	31.8	0.499	4.41	0.566	0.119
Q-1	Quilpie	Medium grey	C	1845	167	3.01	28.9	0.527	4.72	0.598	0.113
Q-1	Quilpie	Light grey-white	C	1972	147	5.61	42.4	0.844	3.86	0.514	0.179
Q-1	Quilpie	Medium grey	C	2021	173	3.49	47.8	0.997	4.86	0.615	0.134
Q-1	Quilpie	Dark grey	C	2053	142	3.20	40.0	0.688	3.66	0.497	0.109
Q-1	Quilpie	Dark grey	C	425	32.9	0.248	22.7	0.177	1.49	0.0513	0.0387
Q-1	Quilpie	Dark grey with brown	C	364	146	0.372	26.7	0.705	4.42	0.303	0.478
Q-1	Quilpie	Light grey	C	328	38.1	0.946	20.7	0.261	1.16	0.0571	0.105
Q-1	Quilpie	Light grey	C	457	129	0.358	40.2	0.693	4.14	0.279	0.390

from which the Mintabie opal formed is unlikely to have been sourced from silica-rich minerals comprising the Whitsunday Volcanics or locally from the Mintabie Beds, which have the lowest CIA values of all opal host rocks (Table 3). The silica may rather have been sourced from the proximal Gawler Craton that comprises Archaean to Mesoproterozoic metasediments, metavolcanics and granitoids (Drexel et al., 1993). Kamber et al. (2005) point out that it would not be unusual for sediment from granite-dominated catchments to have a low Zr/Hf ratio; however, the Zr/Hf ratio of the various granitic rocks within the Gawler Craton range from 35 to 41 (Bryan Schaffler, pers. comm., February 2013). This suggests that the silica fluid from which Mintabie opal formed may have experienced trace element fractionation due to chemical complexation in aqueous media (Bau, 1996) that is significantly less pronounced in other opals from the Great Artesian Basin. Consequently, with the exception of Mintabie opal, it is most likely that the silica fluids from which the opal precipitated were locally derived as speculated by others (Darragh et al., 1966; Thiry and Milnes, 1991; Gaillou et al., 2008) with weathering being the main process driving sedimentary opal formation. Previous studies of opals have reported either their Zr contents (Brown et al., 2004; Rondeau et al., 2010) or Hf contents (McOrist and Smallwood, 1997) but not both elements with the exception of Gaillou et al. (2008) whose analysis yielded Zr/Hf ratios of between

33.9 and 41.5 for Mexican volcanic opals and Brazilian sedimentary opals.

As with most gemstones, not all opals are equal and provenance plays an important role in the quality of the gem and hence its market value. However, there is currently no standardised method of grading opal (Smallwood, 1997) though it is generally accepted that an opal from a particular mining area (e.g., Lightning Ridge black opal) will fetch higher prices than similar looking opal from elsewhere. Once an opal leaves the mine it can be impossible to deduce its origin using visual means. Tracing the provenance of an opal is further complicated by artificial treatments which are applied to opal to enhance its colour (Smallwood, 1997) and make it appear more attractive and valuable than it actually is. Also, since the first synthetic opal was manufactured in 1972 (Smallwood, 2003), high quality imitation opals have flooded the market and many are difficult to recognise using standard gemmological tests (Smallwood, 2003). However, man-made opals usually contain elevated levels of Hf⁺ and Zr⁺ ions (Erel et al., 2003), which occur in very low concentration in natural opals. Therefore, Zr and Hf play a particularly important role in provenance analysis. Consequently, using LA-ICP-MS to determine the concentration of just 4 elements, it is possible to track the provenance of a particular opal to a given mining region and to distinguish it from the synthetic variety

Table 3

Major (wt.%) and trace element (ppm) content of opal host rocks from Coober Pedy, Lightning Ridge, Winton region and Mintabie based on whole rock ICP-MS analysis.

Sample	CP_4	CP_5	W_1A	W_2	W_3	LR_1	LR_2	LR_3	M_1	M_3
Location	Coober Pedy	Coober Pedy	Winton region	Winton region	Winton region	Lightning Ridge	Lightning Ridge	Lightning Ridge	Mintabie	Mintabie
Formation name	Bulldog Shale	Bulldog Shale	Winton Formation	Winton Formation	Winton Formation	Finch Claystone	Finch Claystone	Finch Claystone	Mintabie Beds	Mintabie Beds
SiO ₂	71	94.8	25.2	35.9	36.6	82	86.8	84.4	83.4	80.9
Al ₂ O ₃	15.05	1	3.44	6.95	5.71	9.82	6.09	7.88	8.71	10.35
Fe ₂ O ₃	2.68	0.09	58.6	44.2	44.4	0.82	0.7	0.59	0.48	0.54
MgO	0.5	0.03	0.34	0.29	0.58	0.26	0.18	0.25	0.23	0.27
CaO	0.46	0.15	0.11	0.5	0.26	0.17	0.25	0.25	0.12	0.15
Na ₂ O	1	0.12	0.13	0.08	0.09	0.17	0.35	0.33	0.19	1.53
K ₂ O	0.42	0.07	0.15	0.33	0.18	0.51	0.35	0.33	3.25	4.24
TiO ₂	0.81	0.08	0.21	0.38	0.46	1.13	0.84	1.08	0.74	0.29
MnO	<0.01	<0.01	0.55	0.31	1.04	0.01	0.01	0.01	0.01	0.01
P ₂ O ₅	0.03	0.07	0.53	0.77	0.37	<0.01	0.01	0.01	0.01	0.01
∑	91.95	96.41	89.26	89.71	89.69	94.89	95.58	95.13	97.14	98.29
LOI	7.83	3.59	10.3	9.4	9.35	4.97	4.16	4.73	2.67	1.37
Cr	40	10	100	90	50	80	60	60	30	10
V	292	13	235	150	207	88	75	105	56	22
Co	15	116	52	22	59	6	23	22	14	29
Ni	<1	<1	21	20	59	9	13	13	6	8
Cu	6	8	174	122	50	12	89	79	4	4
Zn	6	8	90	59	148	7	28	14	4	9
Ga	12.5	2	9.1	9.8	11.7	25	12.9	13	10.5	9.8
As	0.4	0.9	8.6	5.2	6.8	0.8	0.7	1.1	0.5	0.5
Se	0.2	<0.2	0.7	1.1	0.8	<0.2	<0.2	<0.2	0.4	0.3
Rb	19.9	6.4	10.4	17.9	9.5	23.8	17.3	17.4	106	135
Sr	146.5	20	47.3	1225	476	44.9	54.3	57.3	101	181
Y	6	1.8	4.9	14.6	10	10.5	8.5	12.6	25.8	8.6
Zr	236	141	41	86	61	266	190	345	790	204
Nb	8.1	1.4	1.7	3.6	3	11.7	6.9	9.1	13.7	5.4
Mo	2	1	3	3	<1	<1	1	<1	<1	<1
Cd	<0.5	<0.5	<0.5	<0.5	<0.5	<0.5	<0.5	<0.5	<0.5	<0.5
Ag	<0.5	<0.5	<0.5	<0.5	<0.5	0.5	<0.5	<0.5	<0.5	<0.5
Sn	8	<1	2	1	1	4	2	3	4	1
Sb	0.12	0.09	0.19	0.15	0.09	0.11	0.16	0.18	<0.05	<0.05
Te	0.02	<0.01	0.06	0.06	0.06	0.02	0.03	0.03	<0.01	0.01
Cs	1.61	1.12	0.87	1.49	0.58	2.21	2.25	2.35	1.89	1.42
Ba	152	27.1	44.6	556	713	163	170	210	1125	1310
La	10.7	3.1	5	79.3	8.3	9.8	9.3	7.9	35.7	20.7
Ce	17	5	7.1	233	22.2	17.6	20.6	18.1	70.8	47
Pr	1.73	0.58	0.79	30.2	2.92	2.08	2.34	2.11	8.39	5.44
Nd	6	2.1	2.9	126	13.1	7.5	8.9	7.6	28.9	18.5
Sm	1.01	0.45	0.66	21.5	3	1.36	1.73	1.61	5.81	3.41
Eu	0.19	0.13	0.17	4.73	0.91	0.32	0.44	0.36	1.59	1.2
Gd	1.08	0.4	0.75	12.15	2.54	1.32	1.56	1.42	4.98	2.19
Tb	0.14	0.05	0.12	1.24	0.34	0.23	0.24	0.26	0.82	0.34
Dy	0.9	0.32	0.79	5.42	1.94	1.66	1.51	1.85	4.83	1.8
Ho	0.2	0.06	0.17	0.76	0.39	0.38	0.33	0.46	0.97	0.33
Er	0.73	0.21	0.59	1.57	1.08	1.23	0.95	1.44	2.68	0.85
Tm	0.13	0.04	0.1	0.21	0.18	0.23	0.16	0.24	0.41	0.15
Yb	0.93	0.23	0.7	1.25	1.2	1.47	1.02	1.57	2.65	0.89
Lu	0.12	0.03	0.1	0.19	0.18	0.27	0.15	0.26	0.44	0.14
Hf	6.8	7.4	1.1	2.7	1.8	8.4	6.3	11.8	23.6	5.8
Ta	0.7	1.5	1.4	0.3	0.2	1	0.8	0.9	1.4	0.9
W	32	416	161	21	27	37	119	99	154	177
Hg	0.023	0.105	0.065	0.028	0.015	0.058	0.039	0.024	0.084	0.11
Tl	<0.5	<0.5	<0.5	<0.5	<0.5	<0.5	<0.5	<0.5	0.5	0.6
Pb	2	4	8	12	10	15	17	18	18	27
Bi	0.12	0.05	0.06	0.06	0.03	0.26	0.16	0.28	0.06	0.03
Th	6.65	2	3.32	4.8	2.45	8.58	8.36	8.42	17.5	5.23
U	1.39	0.59	3.04	2.32	1.16	2.03	1.41	1.6	1.91	0.71
Zr/Hf	34.7	19.1	37.3	31.9	33.9	31.7	30.2	29.2	33.5	35.2
CIA ^a	88.9	88.4	91.5	74.6	89.8	92.0	86.5	89.6	71.0	63.6

^a CIA = [Al₂O₃/(Al₂O₃ + CaO + Na₂O + K₂O)] × 100 where CaO* is the amount of CaO incorporated in the silicate fraction of the rock (Nesbitt and Young, 1982).

with minimal damage to the gemstone. Our approach combining LA-ICP-MS and coupled with multivariate data analysis provides a powerful tool for a wide range of provenance studies, not just gemstones.

5. Conclusions

The combination of LA-ICP-MS analysis and univariate and multivariate statistical approaches provides a powerful and relatively non-

destructive technique for the fingerprinting of opal. It allows the targeting of just 4 elements out of a total of 59 that can be used to track the geographical origin of the opal and provide insights into the opal formation process, particularly into the origin of silica. This methodology can be used to study the provenance of other minerals, metals, archaeological artefacts and rocks where large volumes of data cannot be easily deciphered using ternary plots and principle component analysis. Future elemental analysis of opals will further improve our

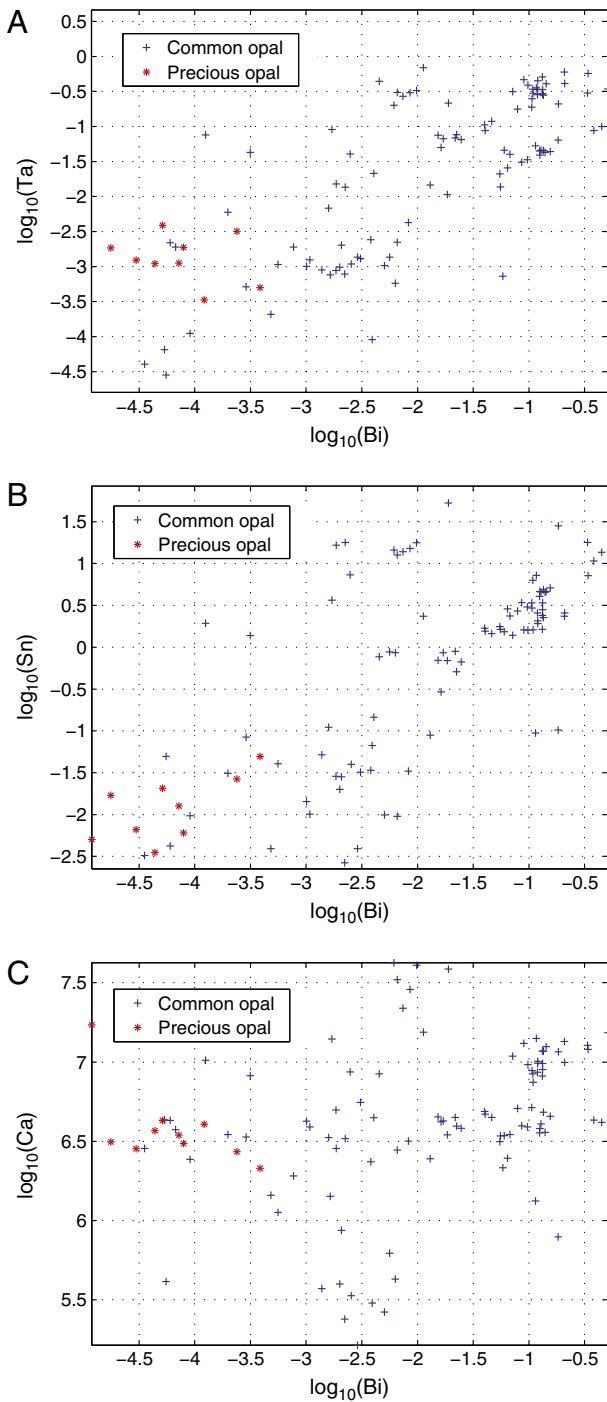


Fig. 5. Distributions of Bi, Ta, Sn and Ca for common and precious opals. This is the best combination of elements by which precious and common opals can be discriminated based on multivariate analysis.

understanding of the chemical variability of different types of opals and will help formulate a robust geological model explaining how sedimentary opal forms.

Acknowledgements

We would like to thank Marcel Guillong and Leonid Danyushevsky from CODES, University of Tasmania for assistance with LA ICP-MS analysis, Mark Raven and Peter Self from CSIRO for XRD analysis. Many thanks to Dietmar Müller, Derek Wyman and two anonymous reviewers for their constructive feedback on the manuscript. We would

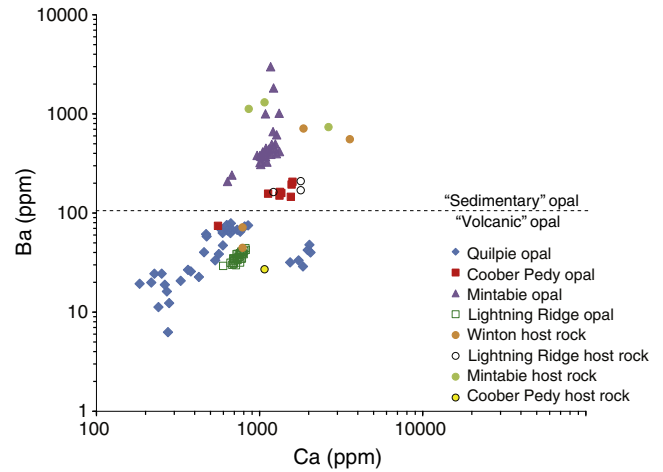


Fig. 6. Ba vs Ca concentrations for opals and associated host rocks from the Great Artesian Basin. The horizontal line denoting the compositional boundary between sedimentary and volcanic opals was taken from Gaillou et al.'s (2008) global study of opals. Ba concentrations above about 110 ppm are expected for opals formed in sedimentary rocks, while those below 110 ppm are expected for opals formed in volcanic rocks. In the Gaillou et al. (2008) study, none of the 7 Australian opals from Lightning Ridge, Mintabie, Quilpie and Coober Pedy have Ba values below 110 ppm.

also like to extend our gratitude to the opal mining community without whose help this study would not have been possible. This project was funded by the Australian Research Council Discovery Grant # DP0987604.

Appendix A. Supplementary data

Supplementary data to this article can be found online at <http://dx.doi.org/10.1016/j.gr.2013.10.013>.

References

- Akahane, H., Furuno, T., Miyajima, H., Yoshikawa, T., Yamamoto, S., 2004. Rapid wood silicification in hot spring water: an explanation of silicification of wood during the Earth's history. *Sedimentary Geology* 169, 219–228.
- Barnes, L.C., Townsend, I.J., Robertson, R.S., Scott, D.C., 1992. Opal: South Australia's Gemstone. Department of Mines and Energy, Geological Survey of South Australia.
- Bau, M., 1996. Controls on the fractionation of isovalent trace elements in magmatic and aqueous systems: evidence from Y/Ho, Zr/Hf, and lanthanide tetrad effect. *Contributions to Mineralogy and Petrology* 123, 323–333.
- Brown, L.D., Ray, A.S., Thomas, P.S., 2004. Elemental analysis of Australian amorphous banded opals by laser-ablation ICP-MS. *Neues Jahrbuch für Mineralogie – Monatshefte* 2004, 411–424.
- Bryan, S.E., Ernst, R.E., 2008. Revised definition of large igneous provinces (LIPs). *Earth-Science Reviews* 86, 175–202.
- Bryan, S., Constantine, A., Stephens, C., Ewart, A., Schön, R., Parianos, J., 1997. Early Cretaceous volcano-sedimentary successions along the eastern Australian continental margin: implications for the break-up of eastern Gondwana. *Earth and Planetary Science Letters* 153, 85–102.
- Bryan, S.E., Ewart, A., Stephens, C.J., Parianos, J., Downes, P.J., 2000. The Whitsunday Volcanic Province, Central Queensland, Australia: lithological and stratigraphic investigations of a silicic-dominated large igneous province. *Journal of Volcanology and Geothermal Research* 99, 55–78.
- Campbell, R.J., Haig, D.W., 1999. Bathymetric change during Early Cretaceous intracratonic marine transgression across the northeastern Eromanga Basin, Australia. *Cretaceous Research* 20, 403–446.
- Claiborne, L.L., Miller, C., Walker, B., Wooden, J., Mazdab, F., Bea, F., 2006. Tracking magmatic processes through Zr/Hf ratios in rocks and Hf and Ti zoning in zircons: an example from the Spirit Mountain batholith, Nevada. *Mineralogical Magazine* 70, 517–543.
- Darragh, P.J., Gaskin, A.J., Terrell, B.C., Sanders, J.V., 1966. Origin of precious opal. *Nature* 209, 13–16.
- Dowell, K., Mavrogenes, J., McPhail, D.C., Watkins, J., 2002. Origin and timing of formation of precious black opal nobbies at Lightning Ridge. *Regolith and Landscapes in Eastern Australia*. 18–20.
- Drexel, J.F., Preiss, W.V., Parker, A.J., 1993. *The Geology of South Australia*. Geological Survey of South Australia, Adelaide.
- Erel, E., Aubriet, F., Finqueneisel, G., Muller, J.F., 2003. Capabilities of laser ablation mass spectrometry in the differentiation of natural and artificial opal gemstones. *Analytical Chemistry* 75, 6422–6429.

- Exon, N.F., Senior, B.R., 1976. The Cretaceous of the Eromanga and Surat Basins. *BMR Journal of Australian Geology and Geophysics* 1, 33–50.
- Frakes, L.A., Burger, D., Apthorpe, M., Wiseman, J., Dettmann, M., Alley, N., Flint, R., Gravestock, D., Ludbrook, N., Backhouse, J., 1987. Australian Cretaceous shorelines, stage by stage. *Palaeogeography, Palaeoclimatology, Palaeoecology* 59, 31–48.
- Gaillou, E., Delaunay, A., Rondeau, B., Bouhnik-le-Coz, M., Fritsch, E., Cornen, G., Monnier, C., 2008. The geochemistry of gem opals as evidence of their origin. *Ore Geology Reviews* 34, 113–126.
- Gallacher, A.D., 2001. *Geochemistry of Sedimentary Opal*, Hebel, Southern Queensland. Ph.D. thesis University of Melbourne.
- Golonka, J., 2007. Phanerozoic paleoenvironment and paleolithofacies maps. *Mesozoic Geology* 33, 211–264.
- Guillong, M., Günther, D., 2001. Quasi 'non-destructive' laser ablation-inductively coupled plasma-mass spectrometry fingerprinting of sapphires. *Spectrochimica Acta Part B: Atomic Spectroscopy* 56, 1219–1231.
- Guillong, M., Danyushevsky, L., Walle, M., Raveggi, M., 2011. The effect of quadrupole ICPMS interface and ion lens design on argide formation. Implications for LA-ICPMS analysis of PGE's in geological samples. *Journal of Analytical Atomic Spectrometry* 26, 1401–1407.
- Iler, R.K., 1979. *The Chemistry of Silica: Solubility, Polymerization, Colloid and Surface Properties and Biochemistry of Silica*. Wiley-Interscience.
- Irber, W., 1999. The lanthanide tetrad effect and its correlation with K/Rb, Eu/Eu*, Sr/Eu, Y/Ho, and Zr/Hf of evolving peraluminous granite suites. *Geochimica et Cosmochimica Acta* 63, 489–508.
- Jochum, K., Seufert, H., Spettel, B., Palme, H., 1986. The solar-system abundances of Nb, Ta, and Y, and the relative abundances of refractory lithophile elements in differentiated planetary bodies. *Geochimica et Cosmochimica Acta* 50, 1173–1183.
- Jones, J.B., Sanders, J.V., Segnit, E.R., 1964. Structure of opal. *Nature* 204, 990–991.
- Kamber, B.S., Greig, A., Collerson, K.D., 2005. A new estimate for the composition of weathered young upper continental crust from alluvial sediments, Queensland, Australia. *Geochimica et Cosmochimica Acta* 69, 1041–1058.
- Liu, H., Motoda, H., 1998. *Feature Selection for Knowledge Discovery and Data Mining*. Kluwer Academic Publishers, Boston.
- Matthews, K.J., Hale, A.J., Gurnis, M., Müller, R.D., DiCaprio, L., 2011. Dynamic subsidence of Eastern Australia during the Cretaceous. *Gondwana Research* 19, 372–383.
- McOrist, G.D., Smallwood, A., 1997. Trace elements in precious and common opals using neutron activation analysis. *Journal of Radioanalytical and Nuclear Chemistry* 223, 9–15.
- Merdith, A.S., Landgrebe, T.S.W., Dutkiewicz, A., Müller, R.D., 2013. Towards a predictive model for opal exploration using a spatio-temporal data mining approach. *Australian Journal of Earth Sciences* 60, 217–229.
- Milliken, K.L., 1989. Petrography and composition of authigenic feldspars, Oligocene Frio Formation, south Texas. *Journal of Sedimentary Research* 59, 361–374.
- Müller, W., Shelley, M., Miller, P., Broude, S., 2009. Initial performance metrics of a new custom-designed ArF excimer LA-ICPMS system coupled to a two-volume laser-ablation cell. *Journal of Analytical Atomic Spectrometry* 24, 209–214.
- Nesbitt, H.W., Young, G.M., 1982. Early Proterozoic climates and plate motions inferred from major element chemistry of lutites. *Nature* 299, 715–717.
- Nesbitt, H.W., Young, G.M., 1984. Prediction of some weathering trends of plutonic and volcanic rocks based on thermodynamic and kinetic considerations. *Geochimica et Cosmochimica Acta* 48, 1523–1534.
- Newberry, T.L., 2004. ⁴⁰Ar/³⁹Ar Geochronology constraints on weathering profile evolution in Australian opal fields. *Australian Geological Convention*. 34.
- Raza, A., Hill, K.C., Korsch, R.J., 2009. Mid-Cretaceous uplift and denudation of the Bowen and Surat Basins, eastern Australia: relationship to Tasman Sea rifting from apatite fission-track and vitrinite-reflectance data. *Australian Journal of Earth Sciences* 56, 501–531.
- Resano, M., Vanhaecke, F., Hutsebaut, D., De Corte, K., Moens, L., 2003. Possibilities of laser ablation-inductively coupled plasma-mass spectrometry for diamond fingerprinting. *Journal of Analytical Atomic Spectrometry* 18, 1238–1242.
- Rondeau, B., Fritsch, E., Mazzero, F., Gauthier, J.P., Cenki-Tok, B., Bekele, E., Gaillou, E., 2010. Play-of-color opal from Wegel Tena, Wollo Province, Ethiopia. *Gems & Gemology* 46, 90–105.
- Sanders, J.V., 1964. Colour of precious opal. *Nature* 204, 1151–1153.
- Segnit, E.R., Stevens, T.J., Jones, J.B., 1965. The role of water in opal. *Journal of the Geological Society of Australia* 12, 211–226.
- Senior, B.R., Mabbutt, J.A., 1979. A proposed method of defining deeply weathered rock units based on regional geological mapping in southwest Queensland. *Journal of the Geological Society of Australia* 26, 237–254.
- Smallwood, A., 1997. A new era for opal nomenclature. *The Australian Gemologist* 19, 486–496.
- Smallwood, A., 2003. 35 years on: a new look at synthetic opal. *The Australian Gemologist* 21, 438–447.
- Smallwood, A.G., Thomas, P.S., Ray, A.S., 2008. Characterisation of the dehydration of Australian sedimentary and volcanic precious opal by thermal methods. *Journal of Thermal Analysis and Calorimetry* 92, 91–95.
- Taylor, S.R., McLennan, S.M., 1985. *The Continental Crust: Its Composition and Evolution*. Blackwell Scientific Publication.
- Thiry, M., Milnes, A.R., 1991. Pedogenic and groundwater silcretes at Stuart Creek opal field, South Australia. *Journal of Sedimentary Research* 61, 111–127.
- Thiry, M., Milnes, A.R., Rayot, V., Simon-Coinçon, R., 2006. Interpretation of palaeoweathering features and successive silicifications in the Tertiary regolith of inland Australia. *Journal of the Geological Society* 163, 723–736.
- Wang, X., Griffin, W., Chen, J., 2010. Hf contents and Zr/Hf ratios in granitic zircons. *Geochemical Journal* 44, 65.
- Zaraisky, G., Aksyuk, A., Devyatova, V., Udoratina, O., Chevychelov, V.Y., 2009. The Zr/Hf ratio as a fractionation indicator of rare-metal granites. *Petrology* 17, 25–45.